

Activity-Dependent Control of Neuronal Output by Local and Global Dendritic Spike Attenuation

Stefan Remy,^{1,*} Jozsef Csicsvari,² and Heinz Beck¹

¹Laboratory for Cognition Research and Experimental Epileptology, Department of Epileptology, University of Bonn, Sigmund-Freud-Strasse 25, D-53105 Bonn, Germany

²MRC Anatomical Neuropharmacology Unit, Department of Pharmacology, University of Oxford, Mansfield Road, Oxford OX1 3TH, UK

*Correspondence: stefan.remy@ukb.uni-bonn.de

DOI 10.1016/j.neuron.2009.01.032

SUMMARY

Neurons possess elaborate dendritic arbors which receive and integrate excitatory synaptic signals. Individual dendritic subbranches exhibit local membrane potential supralinearities, termed dendritic spikes, which control transfer of local synaptic input to the soma. Here, we show that dendritic spikes in CA1 pyramidal cells are strongly regulated by specific types of prior input. While input in the linear range is without effect, supralinear input inhibits subsequent spikes, causing them to attenuate and ultimately fail due to dendritic Na⁺ channel inactivation. This mechanism acts locally within the boundaries of the input branch. If an input is sufficiently strong to trigger axonal action potentials, their back-propagation into the dendritic tree causes a widespread global reduction in dendritic excitability which is prominent after firing patterns occurring *in vivo*. Together, these mechanisms control the capability of individual dendritic branches to trigger somatic action potential output. They are invoked at frequencies encountered during learning, and impose limits on the storage and retrieval rates of information encoded as branch excitability.

INTRODUCTION

How neurons of the central nervous system transform excitatory synaptic inputs to an action potential output signal is the single most important determinant of neuronal function. Most excitatory synapses in cortical principal neurons terminate on thin terminal dendrites that branch off the apical trunk and basal dendrites. In pyramidal neurons, these dendrites are capable of linear, as well as supralinear integration of synaptic input (Cash and Yuste, 1999; Gasparini et al., 2004; Losonczy and Magee, 2006; Schiller et al., 2000). While asynchronous activation of multiple individual synapses causes linear summation, synchronous activation of multiple individual synapses results in a local membrane potential supralinearity, termed dendritic spike (Losonczy et al., 2008; Losonczy and Magee, 2006). This dendritic spike is driven by voltage-gated Na⁺ currents and shaped by the concurrent activa-

tion of NMDA receptors, voltage-gated Ca²⁺ channels and A-type K⁺ currents (Ariav et al., 2003; Losonczy and Magee, 2006; Schiller et al., 2000). If they are sufficiently large, dendritic spikes can trigger a temporally precise action potential output (Ariav et al., 2003). Individual dendritic branches differ in their propensity to generate prominent dendritic spikes and therefore vary in their capability to trigger axonal action potential output (Losonczy et al., 2008). These differential properties appear to be a consequence of branch-specific local plasticity involving voltage-gated ion channels (Losonczy et al., 2008). These findings highlight the role of dendritic branches as independent processing units (Cai et al., 2004; Losonczy et al., 2008; Losonczy and Magee, 2006) previously proposed in modeling studies (Poirazi and Mel, 2001). The critical role of voltage-gated ion channels predicts a strong influence of prior activity on the initiation of dendritic spikes via voltage-dependent inactivation and recovery (Colbert et al., 1997; Jung et al., 1997). Such mechanisms might powerfully affect temporal integration at dendritic branches on time scales of milliseconds to seconds.

RESULTS

We have first tested if prior occurrence of a dendritic spike alters the properties of dendritic spikes subsequently elicited on the same branch. We used multi-site two-photon uncaging to deliver temporally synchronous input to multiple spines located on individual basal dendritic branches of rat hippocampal CA1 pyramidal neurons (Figure 1A; see Experimental Procedures). Increasing the number of stimulated spines initially caused a linear increase in the uncaging-induced excitatory postsynaptic potential (uEPSP), with the sudden appearance of a prominent dendritic spike consisting of a large initial fast, followed by a slower component (Figure 1B). The fast component of the dendritic spike manifested as a large stepwise increase in the first derivation of the voltage trace ($\delta V/\delta t$; Figures 1B and 1C, arrows 1C) that manifested as a prominent supralinearity (Figure 1D, arrows). Branches differed with respect to the magnitude of the stepwise increase in $\delta V/\delta t$ (Example of a “strong” and “weak” branch is depicted in Figures 1B–1D). Two clearly distinct “weak” and “strong” populations of branches could be separated on the basis of the peak $\delta V/\delta t$ of the dendritic spike (Figure 1E; $n = 119$ dendritic branches in 119 cells, 94 “weak” and 25 “strong” branches, see Experimental Procedures for details of classification).

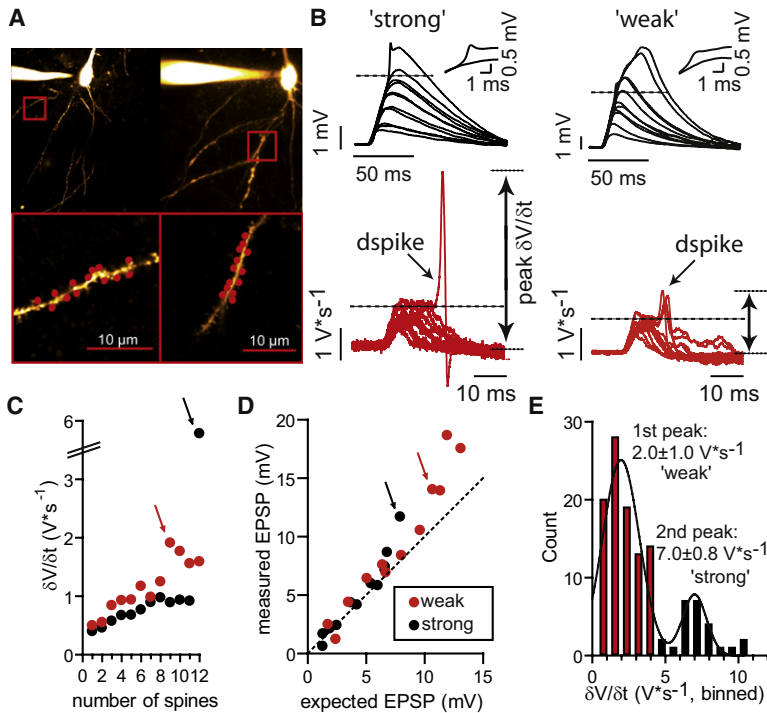


Figure 1. Linear and Supralinear Integration at CA1 Basal Dendrites

(A) Confocal image of two CA1 pyramidal neurons (top) and an individual basal dendrite from each neuron at higher magnification (scale bars 10 μm). Uncaging locations indicated in red. (B) Two-photon uncaging-induced uEPSPs from the left (“strong”) and right (“weak”) basal dendrite in (A) with an increasing number of synchronously activated spines (black, onset phase of the largest uEPSP without a dendritic spike and the first dendritic spike shown in inset). $\delta V/\delta t$ traces shown in red. The dashed line in the upper panels depicts the arithmetic sum of individual uEPSPs and indicates the transition from linear to supralinear signal integration. In the lower panels, the dashed lines represent the last subthreshold $\delta V/\delta t$ values of the compound EPSPs before a dendritic spike was evoked.

(C) Relation of $\delta V/\delta t$ to the number of spines stimulated synchronously. Black and red symbols correspond to the “strong” and “weak” branches shown in (B). The arrows indicate the rapid increase in $\delta V/\delta t$ associated with the occurrence of the first dendritic spike.

(D) Plot of the measured uEPSP peak voltage versus the expected EPSP calculated as the arithmetic sum of the uEPSPs obtained by stimulation of the individual spines. Arrows indicate the point at which deviation from linearity occurred.

(E) Distribution of branches according to the degree of dendritic nonlinearity quantified as the peak $\delta V/\delta t$. The line corresponds to a fit with the sum of two Gaussian equations (see [Experimental Procedures](#)).

Supralinear Integration Induces Dendritic Spike Attenuation

CA1 pyramidal neurons receive synchronized inputs at theta frequencies ranging from 5 to 10 Hz during behavior (Buzsaki, 2002). We therefore tested if dendritic spikes are systematically altered at these frequencies. At 1 Hz, changes in peak $\delta V/\delta t$ were small (reduction to $85\% \pm 6\%$ during 5 stimulations; Figure 2A). At 5 and 10 Hz, however, a strong reduction of the fast component of the dendritic spike was observed during the 5 stimulus train (reduction of peak $\delta V/\delta t$ to $61\% \pm 6\%$ and $43\% \pm 6\%$, respectively, $n = 8$ branches in 8 cells; Figures 2A and 2B). “Strong” branches showed a significantly stronger attenuation during 5 Hz stimulation (Figure 2C), with a reduction of peak $\delta V/\delta t$ to $29\% \pm 6\%$ during 5 stimulations ($n = 6$ branches from 6 cells, compared to $57\% \pm 4\%$ in weak branches, $n = 18$ branches from 18 cells, $p < 0.01$; Figure 2D). The attenuation induced by dendritic spikes lasted for several hundred milliseconds (Figure 2E, $n = 9$ –11 branches from 8 neurons). Variation of input synchronization did not result in differences in dendritic spike attenuation ratio observed with a 200 ms interpulse interval (ratio at 1 ms uncaging dwell time: 0.74 ± 0.09 , 0.5 ms: 0.69 ± 0.08 , 0.2 ms dwell time: 0.75 ± 0.04 , $n = 6$, n.s., repeated-measures ANOVA).

During the inactivating train, we noted that the progressive attenuation of the fast initial component was not immediately associated with a reduction of the slow component of the dendritic spike (Figure 2F, black traces). However, upon failure of the fast dendritic spike component (fifth stimulation; Figure 2F, black traces, $\delta V/\delta t$ shown in red traces) the slow spike component was invariably absent. As a consequence, in both “weak” and “strong” branches, the failure of the fast component

of the dendritic spike was associated with a significant reduction of the area under the uncaging-induced voltage change (Figure 2G). This is consistent with the idea that a fast Na^+ spike is required for the subsequent slow depolarization mediated by NMDARs and other voltage-gated currents (Ariav et al., 2003; Losonczy and Magee, 2006). The failure of dendritic spikes during a stimulus train suggests a conversion of these branches to a linear processing mode. We tested this idea by calculating the ratio of measured uEPSP to the expected EPSP obtained as the arithmetic sum of the uEPSPs at the individual contributing spines. This ratio changed from 1.49 ± 0.28 and 1.52 ± 0.16 at the beginning of a stimulus train to 0.99 ± 0.07 and 1.11 after failure of the dendritic spike ($n = 6$ “weak” branches, $n = 2$ “strong” branches, respectively), indicating conversion to a linear processing mode.

Does subthreshold activity in the linear range also depress branch excitability by reducing subsequent dendritic spikes? To address this question, we induced dendritic spikes with and without a preceding uEPSP evoked on the same branch (Figure 3A, lower trace, numbers in parentheses indicate the number of stimulated spines). uEPSPs of different magnitudes were not effective in attenuating dendritic spikes as revealed by the lack of change in $\delta V/\delta t$ (Figure 3A, lower panel, $\delta V/\delta t$ shown in red, summarized in Figure 3B; $n = 8$ weak and $n = 3$ strong branches from different cells). Thus, supralinear integration by dendritic spikes on an individual branch, but not a uEPSP, promotes a temporary conversion of the same branch to a linear processing mode.

We next tested if synaptically evoked dendritic spikes display a similar attenuation using focal electrical stimulation (see [Experimental Procedures](#); Figure 4A). Increasing the stimulation

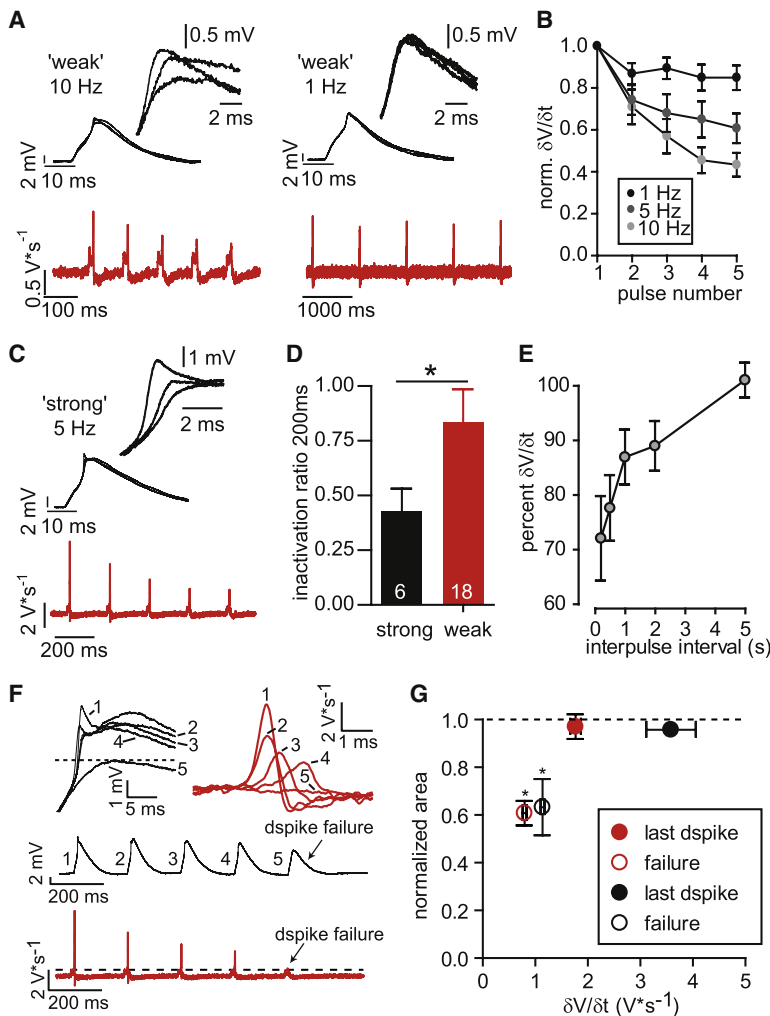


Figure 2. Supralinear Integration Causes a Reduction of Subsequent Dendritic Spikes at Individual Branches

(A) Attenuation of dendritic spikes during repetitive stimulation at 10 Hz (left, black traces, larger magnification in inset) is reflected in a progressive reduction of peak $\delta V/\delta t$ (red traces). Such an attenuation is not seen at 1 Hz (right).

(B) Quantification during a train of five stimulations.

(C and D) Significantly more attenuation is seen in “strong” branches (inactivation ratio = $\delta V/\delta t$ second dspike/first dspike, numbers in bars represent numbers of branches from different cells, $p < 0.01$, example in [C], quantification in [D]).

(E) Analyzing different time intervals of dendritic spikes (100 and 200 ms, 1 s) revealed that the attenuation induced by the initial dendritic spike lasts for several hundred milliseconds.

(F) The slow component of dendritic spikes is reduced only when the fast initial component fails. Representative example shows reduction of the fast component during a 5 Hz stimulation train (evidenced by the reduction in $\delta V/\delta t$, in red, at higher magnification in the inset) until the dendritic spike fails (fifth stimulation, indicated by numbers). The dashed line indicates the $\delta V/\delta t$ values obtained for the expected EPSP calculated as arithmetic sum of the individual spine uEPSPs. The inset (top left) clearly shows that failure of the fast component of the dendritic spike causes a sudden reduction in the slow component.

(G) Quantification of this observation by determining the area under the voltage trace for the last uEPSP with a superimposed spike, and the first uEPSP with failure of the dendritic spike. Black and red symbols correspond to “strong” and “weak” spikes, respectively. Asterisks indicate significant difference. Error bars indicate standard error of the mean (SEM).

intensity initially resulted in a monotonous increase in the size of the stimulation-evoked EPSP (sEPSP), with a sudden appearance of a dendritic spike in 12 of 19 experiments (Figure 4B, black traces, $\delta V/\delta t$ shown in red traces). As described for uEPSPs, the dendritic spike manifested as a stepwise increase in the maximal $\delta V/\delta t$ of the voltage trace (red in Figures 4B and 4C). We next elicited sEPSP-driven dendritic spikes repetitively at frequencies of 1, 5, and 10 Hz (Figure 4D). In these experiments, occurrence of a dendritic spike invariably caused reduction of a subsequent dendritic spike, or its failure (Figure 4E, example shown for 5 Hz stimulation frequency, red traces in the inset show $\delta V/\delta t$ for the traces indicated). These experiments are potentially complicated by facilitation or depression of sEPSPs during repetitive stimulation. We tested this issue by applying synaptic stimulations that elicited sEPSPs but were subthreshold for dendritic spikes. These experiments revealed a transient facilitation of sEPSPs at 10 Hz (second stimulation: $126.8\% \pm 9.6\%$ of first EPSP amplitude; third stimulation $123.5\% \pm 9.3\%$ of first EPSP amplitude, both $p < 0.05$) but not at 5 or 1 Hz (Figure 4F). Thus, nonuniform size of sEPSPs during stimulation trains is unlikely to account for dendritic spike attenuation observed at 5 or 1 Hz. The spike attenuation is quantified for pairs of consecutive dendritic spikes

nonconsecutively (Figure 4G, black data points). Overall, these data indicate that spike attenuation is also observed when spikes are initiated via synaptic release of glutamate.

Local and Global Mechanisms for Dendritic Spike Attenuation by Prior Activity

Is the attenuation of subsequent spikes limited to the input branch, or does it also affect adjacent dendritic branching off the same parent dendrite? To address this issue, we elicited dendritic spikes on two daughter branches (Figure 5A, stimulated spines indicated by red and blue dots) and tested the interaction between them. At each individual branch, dendritic spikes caused prominent inactivation of following dendritic spikes (Figure 5B, stimulated branch indicated by red and blue dots, 200 ms interval, $\delta V/\delta t$ change on average $-34\% \pm 6\%$, $n = 16$, $\delta V/\delta t$ shown in red). In contrast, a dendritic spike in one daughter branch did not significantly alter a subsequent spike in the other daughter branch from the same parent dendrite (Figure 5C; $\delta V/\delta t$ change on average $0.5\% \pm 2.0\%$, $n = 16$ branches from 8 cells, mean distance $58 \pm 8 \mu\text{m}$). This indicates that dendritic spikes cause a branch-specific, local attenuation of subsequent spikes.

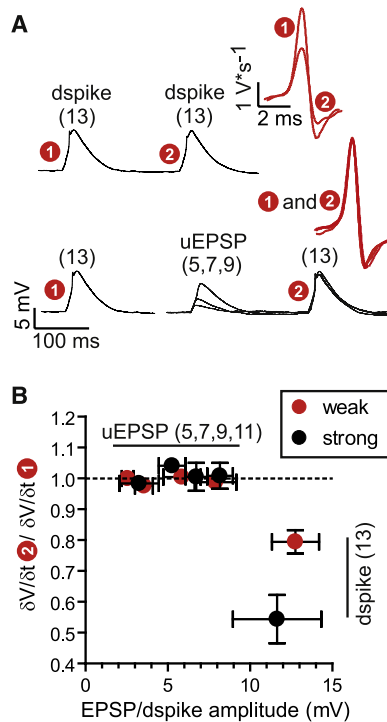


Figure 3. Linear Integration on Individual Branches Does Not Cause Dendritic Spike Attenuation

(A) Induction of dendritic spikes with and without a preceding uEPSP evoked on the same branch (lower trace). $\delta V/\delta t$ at larger magnification (red traces) reveal no change in dendritic spikes, but $\delta V/\delta t$ is strongly attenuated by prior occurrence of a dendritic spike (upper traces). Number of synchronously activated spines indicated in parentheses.

(B) Inactivation ratio computed as the ratio of $\delta V/\delta t$ with a preceding uEPSP/spike and $\delta V/\delta t$ without preceding activity. With preceding uEPSPs, no attenuation of dendritic spikes is seen in “weak” and “strong” branches even for large uEPSPs, but preceding dendritic spikes cause attenuation. Error bars indicate standard error of the mean (SEM).

Dendritic spikes are capable of triggering somatic action potentials (Ariav et al., 2003; Golding and Spruston, 1998) which then invade the basal and apical dendritic arborizations. They could therefore cause a global reduction of dendritic excitability. Indeed, dendritic spikes were strongly attenuated both by action potential bursts (Figure 5D, uncaging locations indicated by blue dots, 200 ms interval between action potential and uncaging stimuli, $\delta V/\delta t$ change on average $-48\% \pm 8\%$, $n = 16$ branches from 13 cells) and by single action potentials elicited with somatic current injection (Figure 5E, $\delta V/\delta t$ change on average $-19\% \pm 5\%$, $n = 9$ branches from 9 cells). Importantly, this attenuation was observed in all dendrites, including pairs of daughter dendrites emanating from the same parent dendrites ($n = 6$ pairs, sister dendrite to Figures 5D and 5E shown in Figures 5F and 5G). Attenuation could also be observed when somatic action potentials were triggered by a dendritic spike (Figure 5G; $n = 23$). This indicates that attenuation of dendritic spikes by axonally generated action potentials back-propagating into dendrites is a global plasticity mechanism that affects most dendritic branches. This mechanism contrasts with the local, branch-specific attenuation induced by dendritic spikes. The attenuation induced by either

an action potential, or an action potential burst lasted for several hundreds of milliseconds, similar to the attenuation caused by individual dendritic spike (Figure 5H, cf. Figure 2E).

Activity-Dependent Spike Attenuation Influences Action Potential Output

The results above predict that attenuation of dendritic spikes either by local or global inactivation will reduce the likelihood of the corresponding branches to elicit an action potential output. We tested this idea by eliciting a dendritic spike on a branch at sufficient strength to elicit a somatic action potential (Figure 6A, left panel). Preceding the uncaging stimulus with an action potential burst led to reduction of the dendritic spike and failure of action potential generation (“2” in Figure 6A; $n = 12$). A similar finding was obtained with single action potentials ($n = 6$, data not shown). We also examined the effects of repetitive stimulation on the capability of individual branches to trigger neuronal action potential output. Repetitive uncaging (5 Hz) caused an initially present action potential to fail during the stimulation train (Figures 6B and 6C; $n = 15$). In those neurons that generated two or more somatic action potentials to repetitive stimulation, we also observed a systematic variation of the timing of these action potentials. At the first stimulation in a train, a somatic action potential with a precise timing was elicited by the fast component of the dendritic spike (indicated by “2” in Figure 6B; see Ariav et al., 2003). At subsequent stimulations in a train, the fast component was progressively reduced. In these cases, the slower component of the dendritic spike often initiated a somatic action potential (indicated by “2” in Figure 6B), resulting in a systematically longer delay to initiation of the action potential (Figure 6D). Thus, repetitive synchronous activation causes not only a gradual failure of action potential output, but also a systematic change in spike timing. These results indicate that synaptic input sub-threshold for dendritic spikes does not change dendritic supralinear integration (Figure 6E, left panel), whereas dendritic spikes strongly inhibit supralinear integration in the stimulated branch only (Figure 6E, middle panel). Somatic action potentials cause a more global attenuation of dendritic spikes (Figure 6E, right panel).

Back-propagating action potentials will cause Na⁺ channel inactivation in both the stimulated branch, as well as all lower-order parent dendrites. This raises the question whether back-propagating action potentials attenuate dendritic spikes via an action on the parent branches or on the stimulated branch. We therefore examined whether back-propagating action potentials induce spike attenuation at both proximal and distal locations on the same basal dendritic arbor (see Figure S2A available online). Of 20 experiments in which stimulation was performed on proximal and distal locations, dendritic spikes in both locations could be observed only in four cases. In these, dendritic spike attenuation by prior action potentials was observed in all cases at both proximal ($\delta V/\delta t$ change on average $-27\% \pm 11\%$) and distal ($\delta V/\delta t$ change on average $-26\% \pm 6\%$) locations (Figures S2C and S2E). The same held true for action potential bursts, which induced more potent attenuation at proximal and distal locations ($-47\% \pm 14\%$ burst of 3 APs at proximal and $-40\% \pm 14\%$ burst of 3 APs at distal locations, respectively; Figures S2B and S2D). We note that a quantitative interpretation is difficult, because proximal locations invariably yielded strong spikes, which

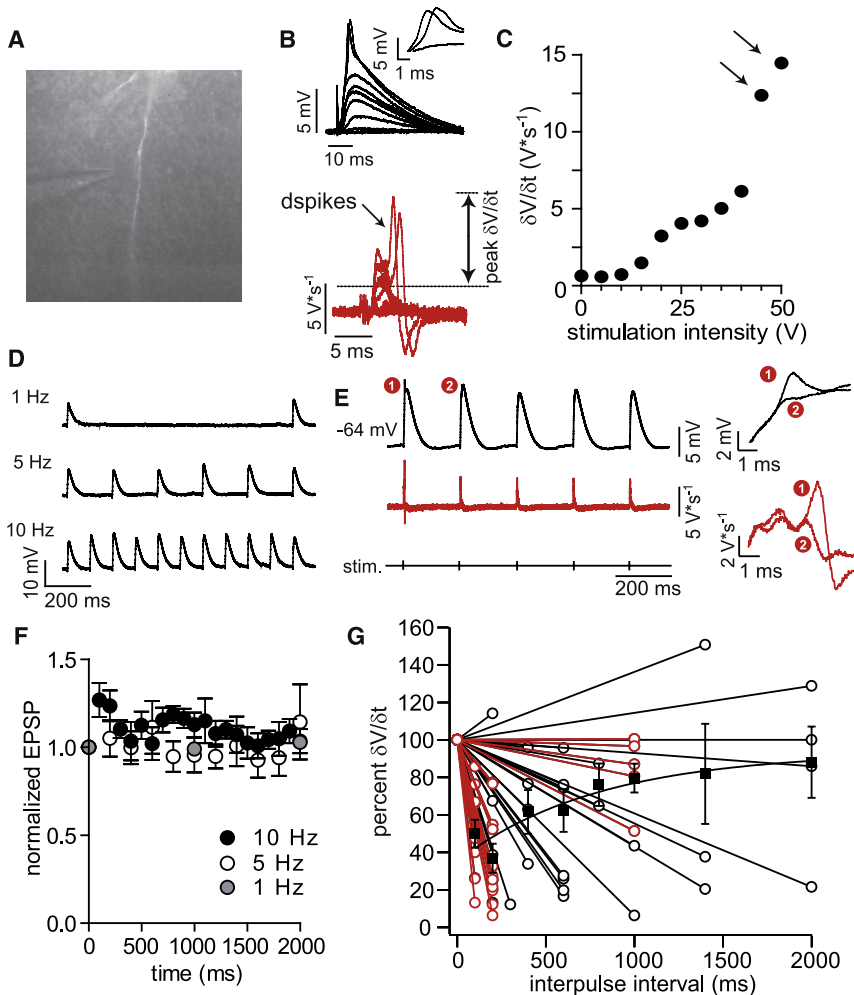


Figure 4. Synaptically Evoked Dendritic Spikes Display Spike Attenuation

(A) A stimulation electrode was placed close to a basal dendrite to electrically stimulate synaptic input.

(B and C) Increasing the stimulation intensity initially resulted in a monotonous increase in the size of the stimulation-evoked EPSP (sEPSP), with a sudden appearance of a dendritic spike (black traces, dendritic spikes and largest sEPSP shown magnified in inset, $\delta V/\delta t$ shown in red traces). The stepwise increase in the maximal $\delta V/\delta t$ when dendritic spikes occurred are indicated with arrows in (C).

(D and E) Representative sEPSP-driven dendritic spikes elicited at frequencies of 1, 5, and 10 Hz, example shown for 5 Hz stimulation frequency in (E) (red traces in the inset show $\delta V/\delta t$ for the traces indicated).

(F) Dynamics of sEPSPs during repetitive stimulation. A transient facilitation of sEPSPs occurs at 10 Hz, but not at 5 or 1 Hz.

(G) The spike attenuation is quantified for pairs of consecutive dendritic spikes occurring during stimulation trains for 10, 5, and 1 Hz (interstimulus intervals of 0.1, 0.2, and 1 s, red data points, pairs of spikes connected by lines). These recordings invariably revealed a strong attenuation of dendritic spikes. This also held true when spikes during stimulation trains were analyzed that occurred nonconsecutively (black data points, spikes from individual trains connected by lines). Averaging spike amplitudes with different ISIs revealed a slow recovery of spike attenuation (filled squares). Error bars indicate standard error of the mean (SEM).

attenuate strongly, whereas distal locations yielded weak spikes, which show weak attenuation (cf. Figure 2D). Thus, a direct comparison of proximal versus distal input locations is difficult.

Mechanism of Spike Attenuation

We next addressed potential mechanisms underlying dendritic spike attenuation. A prominent slow inactivation of Na⁺ channels has been described in CA1 apical dendrites (Colbert et al., 1997; Jung et al., 1997), but it is unclear whether smaller caliber dendrites such as radial oblique or basal dendrites display a similar phenomenon. We have directly recorded Na⁺ currents from basal dendrites in the cell-attached configuration (see Experimental Procedures). When repetitively elicited with brief depolarizing pulses (Figure 7A, inset), Na⁺ currents displayed prominent inactivation at 5 Hz (Figure 7B, upper panel shows superimposed current traces, lower panel shows continuous current recording during the stimulation train). Na⁺ current amplitude was gradually reduced to 69% ± 3% during a train of 10 stimulations at 5 Hz (n = 8; see Figure 7B). No significant rundown of Na⁺ currents was observed during these recordings.

In addition to Na⁺ currents, dendritic A-type K⁺ currents have also been shown to modulate the size of dendritic spikes

(Losonczy et al., 2008). Blocking A-type K⁺ currents with 4-aminopyridine (2 mM) resulted in a transition of the intrinsic firing mode of CA1 neurons from regular- to burst-firing, as previously described (Magee and Carruth, 1999; n = 9; see inset, Figure 7C), confirming the efficacy of the 4-aminopyridine application. At the same time, an increase in the $\delta V/\delta t$ of dendritic spikes was observed (Figure 7C, red traces; quantification in Figure 7D; increase by 20.5% ± 8.7%, n = 7, p < 0.05). These changes were not, however, accompanied by altered dendritic spike attenuation (see insets of Figure 7C for superposition of magnified $\delta V/\delta t$ traces; quantification in Figure 7E). These data suggest that A-type K⁺ currents modulate the size of dendritic spikes, as previously described (Losonczy et al., 2008), but not their dynamics during repetitive activity patterns. They also imply a role for slow inactivation of dendritic Na⁺ channels in spike attenuation, although they do not exclude an additional role of other ion channels. Modest variation of the holding potential did not affect spike attenuation (see Figure S3 and legend).

Spike Attenuation Induced by In Vivo Activity Patterns

We next began to evaluate the relevance of spike attenuation for the in-vivo situation. CA1 neurons receive synchronous input

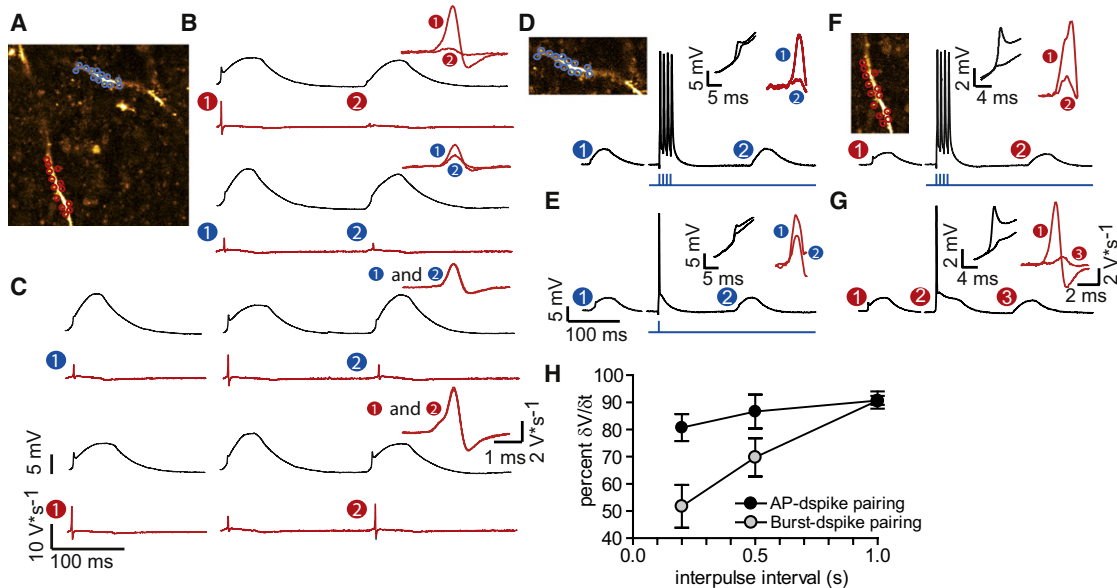


Figure 5. Local versus Global Attenuation of Dendritic Spikes

(A) Confocal image of two adjacent dendritic branches bifurcating from the same parent dendrite. Uncaging locations on the two daughter branches indicated in red and blue.

(B) Dendritic spikes elicited by synchronous uncaging on either of the two daughter branches, location of uncaging indicated by blue or red circles. Red traces correspond to $\delta V/\delta t$, traces indicated by numbers shown at larger magnification and superimposed on the right ($\delta V/\delta t$ shown in red).

(C) Stimulation of one daughter branch either in isolation, or preceded by a stimulation in the other daughter branch as indicated.

(D and E) Attenuation of dendritic spikes by somatic action potentials. Dendritic spikes were elicited by synchronous activation of the sites shown (inset) either in isolation (left) or following an action potential burst (D) or single action potential (E) elicited by somatic current injection. Voltage traces (black) as well as $\delta V/\delta t$ (red) shown at large magnification in the inset indicate powerful attenuation of dendritic spikes.

(F and G) Similar experiment on the sister dendrite to Figures 4D and 4E. In (G), the somatic action potential was elicited by the dendritic spike, with similar results. Attenuation of dendritic spikes by somatically generated action potentials back-propagating into dendrites is a global plasticity mechanism that affects most dendritic branches whereas attenuation by dendritic spikes is local.

(H) Time course of dendritic spike attenuation either by a preceding dendritic spike, a somatic action potential, or an action potential burst. Error bars indicate standard error of the mean (SEM).

likely to trigger dendritic spikes in particular during sharp waves/ripple (SWR) patterns. Dendritic spikes have indeed been observed under SWRs (Kamondi et al., 1998). The occurrence of dendritic spikes during SWRs is also facilitated by the strong 5- to 7-fold increase of network synchronization of CA1 and CA3 pyramidal cells leading to 15% CA3 and 30% of CA1 pyramidal cells to fire action potentials in an SWR event (Csicsvari et al., 2000; Gasparini and Magee, 2006). Although most SWRs tend to occur during immobility and slow wave sleep, they also occur in active waking periods when hippocampal pyramidal cells also fire in relation to space. These exploration-associated SWRs (eSWRs) have been suggested to have role in neuronal plasticity related to storage of new place maps and to the reactivation of such place maps in sleep (O'Neill et al., 2006; Cheng and Frank, 2008). We therefore recorded single-unit activity from $n = 151$ CA1 pyramidal cells that exhibited place-related firing while the animal has been actively exploring either familiar or novel environments (Figure 8A). We selected activity periods that contained an eSWR when the animal was within and outside of their place fields (Figure 8B). We then analyzed the patterns of single unit activity in a 1 s time period before onset of the eSWRs. These patterns proved to be variable. First we examined the time interval between eSWR onset and the last spike that occurred

before that to test how often the last spike is expected to be able to block dendritic spikes during eSWRs. As expected, because of the increased firing probability of cells, the incidence of short (<100 ms) time intervals was higher (Figure 8C). Moreover, the number of spikes in the 1 s interval preceding eSWRs was lower outside place fields (Figure 8D).

We chose representative *in vivo* recordings containing either 2, 4, or 6–8 spikes in the 1 s period before onset of the eSWR ($n = 36$ examples of trains). We then induced the same temporal sequence of action potentials in CA1 pyramidal neurons *in vitro* by applying somatic current injections (3 ms, 1–1.5 nA; Figure 8D, see examples of spike trains in leftmost panel; $n = 11$ cells, $n = 5$ –8 examples for each condition, $n = 196$ spike trains applied, $n = 2$ –5 repetitions per single spike train example). We induced dendritic spikes after the action potential trains and compared them to a dendritic control spike elicited before the action potential train (Figure 8E, right panel). This allowed us to quantify the amount of spike attenuation produced by action potential trains similar to *in vivo* activity patterns (Figure 8F; $\delta V/\delta t$ of the posttrain dendritic spike divided by the $\delta V/\delta t$ of the control spike). These experiments revealed that even in those cases in which only two somatic action potentials occurred during the 1 s time window preceding eSWRs, dendritic spikes

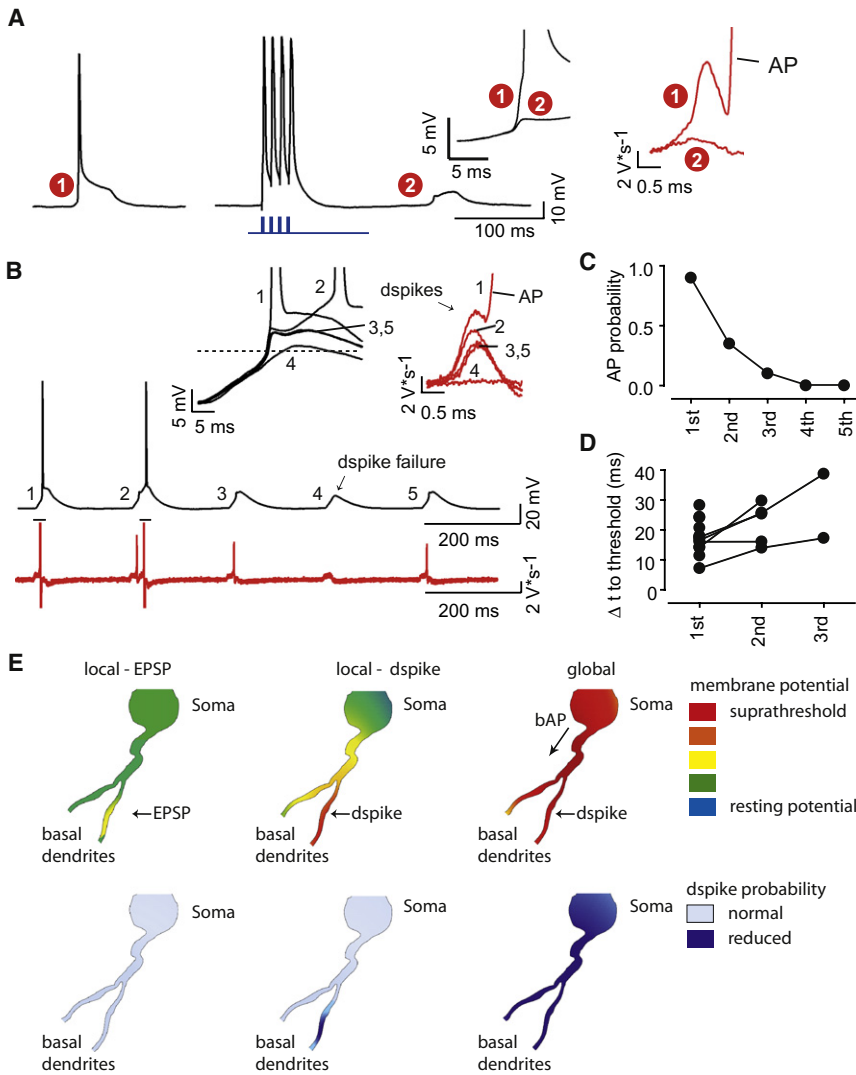


Figure 6. Reduction of Action Potential Output by Dendritic Spike Attenuation

(A) Representative experiment in which the first uEPSP elicited a dendritic spike sufficiently large to trigger a somatic action potential (black trace, 1). Preceding the uEPSP with an action potential burst elicited by somatic current injection (indicated by blue traces) caused a reduction of the dendritic spike and concomitant failure of action potential generation (2, see inset for magnified and superimposed traces 1–2). (B) Representative experiment in which the first stimulation in a train elicits a dendritic spike which triggers a somatic action potential (see inset, trace 1 for higher magnification, $\delta V/\delta t$ traces in red). The second uEPSP elicited an action potential via the slow phase of the dendritic spike (trace 2). At further stimulations, somatic action potential generation failed (traces 3–5, see inset for higher magnification). (C) Probability to generate an action potential during the first to fifth stimulation in a train for those branches that were capable of generating an action potential during the train. (D) Delay between onset of the uncaging stimulation and the onset of the somatic action potential during a stimulus train. (E) Schematic diagram of local versus global spike attenuation mechanisms.

were strongly attenuated. This did not appear different for spike trains recorded inside or outside the place field of the respective CA1 neuron (Figure 8F). Thus, spike trains with a similar number of action potentials from inside and outside the place field did not produce differential effects, but the probability that cells fire >2 spikes before an SWR was higher inside the place field. Thus, dendritic spike attenuation during an eSWR is more likely to occur inside the place field. Second, cells that fire at high frequencies at the center of their SWRs are expected to show even stronger dendritic spike attenuation. These results indicate that global dendritic spike attenuation occurs in a substantial portion of CA1 pyramidal neurons in vivo.

DISCUSSION

These results demonstrate that supralinear integration at basal dendrites is strongly dependent on past neuronal activity. Synaptic input that is not sufficiently strong or synchronous to elicit a dendritic spike does not cause a change in the dendritic capacity for supralinear integration (Figure 6E, left panel). In

contrast, synchronous input that elicits a dendritic spike strongly inhibits supralinear integration only in the stimulated branch for several hundred milliseconds (Figure 6E, middle panel). When synchronous input is strong enough to elicit an action potential at the initial segment, action potential back-propagation into the dendritic arbor causes a more global attenuation of dendritic spikes in all dendrites (Figure 6E, right panel; see also Golding and Spruston, 1998). This global mechanism is likely invoked by patterns of action potentials occurring in-vivo, in a substantial subpopulation of CA1 neurons.

Our data do not allow us to conclude that this attenuation is different at proximal versus more distal input locations. However, it is likely that this mechanism depends strongly on the local amplitude of the back-propagating action potential. Accordingly, it may be less active in distal dendrites, because the action potential amplitude is attenuated to a varying extent with increasing distance from the soma (Golding et al., 2001; Kampa and Stuart, 2006; Nevian et al., 2007; Spruston et al., 1995; Zhou et al., 2008). Additionally, changes in voltage-gated channels that affect action potential back-propagation, for instance A-type K^+ currents (Hoffman et al., 1997) would be expected to affect dendritic spike attenuation. Dendritic spike attenuation was more pronounced following an action potential burst, compared to a single somatic action potential. This finding is expected because of the more prolonged dendritic depolarization elicited by an action potential burst. This dendritic

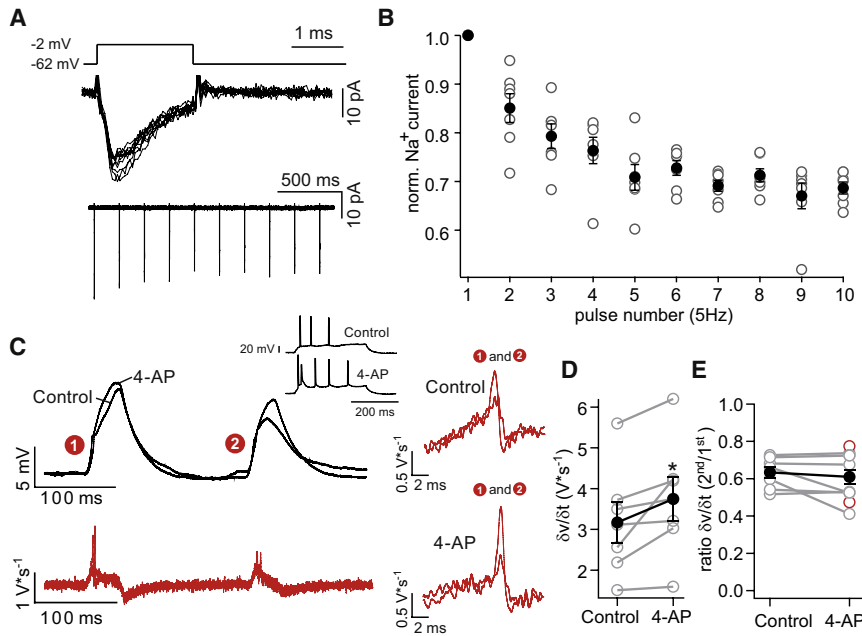


Figure 7. Mechanisms Underlying Dendritic Spike Attenuation

(A) Direct recordings of Na^+ currents from basal dendrites in the cell-attached configuration (see [Experimental Procedures](#)). Inset: upper panel shows superimposed current traces, lower panel shows continuous current recording during a 5 Hz stimulation train with 10 stimulations.

(B) Reduction of Na^+ current amplitude during 5 Hz stimulation trains. Empty circles represent individual experiments, black circles represent average values.

(C) Role of A-type K^+ currents. Representative experiment in which dendritic spikes were elicited under control conditions, and after application of 2 mM 4-AP. Application of 4-AP resulted in a transition of the intrinsic firing mode of CA1 neurons from regular to burst firing (inset, firing elicited by somatic current injection, duration 300 ms, 500 pA). Black traces correspond to voltage traces, red traces correspond to $\delta V/\delta t$ traces. Right panels show superposition of magnified $\delta V/\delta t$ traces at the time points indicated by number (1 + 2).

(D) Quantification of the change in $\delta V/\delta t$ upon application of 4-aminopyridine. Significant difference indicated by asterisk.

(E) Quantification of spike attenuation. Attenuation

was calculated as the ratio of the maximal $\delta V/\delta t$ of the first versus the second of two spikes separated by 200 ms. In (D) and (E), empty circles represent individual experiments, black circles represent average values. The red circles in (E) correspond to recordings in which 4-aminopyridine was present during the whole experiment. Averages are only of experiments in which 4-aminopyridine was washed in. Error bars indicate standard error of the mean (SEM).

depolarization may also be strongly enhanced by voltage-gated Na^+ and Ca^{2+} channels, causing increased dendritic spike attenuation (Kampa and Stuart, 2006; Letzkus et al., 2006; Stuart et al., 1997). Thus, pyramidal cell basal dendrites implement two mechanisms of temporal integration, one active within the boundaries of individual dendritic branches (local), and the other affecting larger populations of dendrites, dependent on the properties of action potential back-propagation (global).

The mechanism of local spike attenuation is likely a use-dependent attenuation of Na^+ currents, demonstrated by direct patch-clamp recordings from basal dendrites. At the same time, A-type K^+ channels do not appear to play a major role in dendritic spike attenuation, even though they modify the firing mode of CA1 neurons, and increase the overall $\delta V/\delta t$ of dendritic spikes (see also Magee and Carruth, 1999; Losonczy et al., 2008). This finding is interesting, because it enables dendrites to modify dendritic spike magnitude via plasticity of A-type currents (Losonczy et al., 2008) without affecting the temporal dynamics of spike attenuation during theta-patterned stimulation.

What is the purpose of activity-dependent attenuation of dendritic spikes? It is helpful to consider this mechanism in the light of the following question: what is the pattern of synaptic input that is most likely to elicit an action potential output? Clearly, the ideal afferent activity pattern would be a rare, highly synchronous input in the supralinear range, superimposed on a background activity in the linear range. In contrast, frequently occurring synchronized activity in the supralinear range would cause local attenuation of dendritic spikes that limits the capability of individual branches to cause somatic action potential output. This scenario changes if a dendritic spike successfully initiates a somatic action potential. In this case, most dendritic

branches will be temporarily rendered less effective in initiating an action potential output. These mechanisms may be viewed as branch-specific versus global temporal integration mechanisms active within the time domain of common neuronal rhythmic forms of activity such as theta activity. In particular, the application of action potential patterns derived from *in vivo* recordings reveal that global dendritic spike attenuation is prominent at transitions of theta activity to SPWs. Depending on the pattern of pre-SWR neuronal activity, the extent of dendritic spike attenuation may vary for different behavioral contexts, as shown for pre-SWR action potential trains derived within and outside of place fields (see [Figure 8](#) and [Results](#) section). This may also have a bearing on other behavioral states. For instance, the mean firing rates of CA1 pyramidal neurons are significantly higher during pre-SWR theta activity when compared to non-SWR slow-wave sleep (O'Neill et al., 2006), implying less dendritic spike inactivation in the latter condition.

Interestingly, dendrites lacking voltage-gated Na^+ channels (Stuart and Häusser, 1994) utilize a different mechanism that serves to reduce excitability following dendritic spikes. In cerebellar Purkinje cells, for instance, dendritic Ca^{2+} spikes trigger a local endocannabinoid-dependent downregulation of excitatory input (Rancz and Häusser, 2006).

Plastic upregulation of the degree of supralinearity exhibited by individual branches has been proposed as a mechanism to store uniquely correlated input patterns to individual branches (Losonczy et al., 2008), because the subsequent stimulation of the same branch with a correlated input would be much more likely to evoke a temporally precise action potential output. Our results imply that the retrieval of information in this system requires activity to be sparse in order to prevent significant

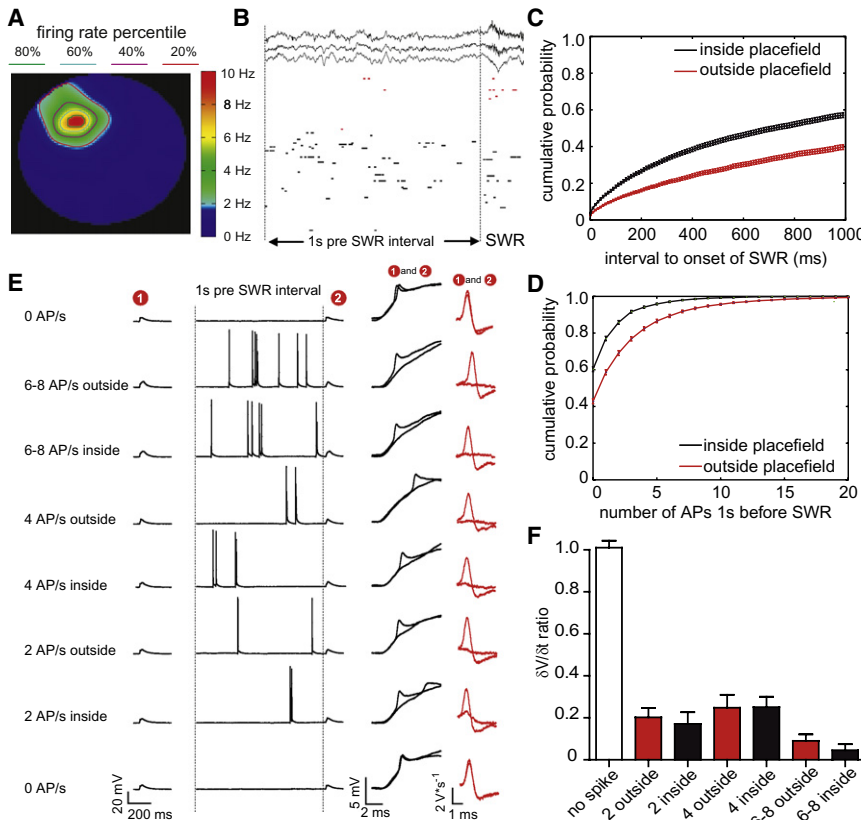


Figure 8. Blockade of Dendritic Spikes by Using In Vivo Spike Trains

(A) Place-rate map of a representative place cell. The animal was exploring a circular arena, thus black regions mark locations outside the arena that the animal never visited. Contour lines mark firing rate levels as 20, 40, 60, 80 percentile relative to the maximum rate. Areas that were inside the 20% of the contour lines marked the place field of the cell.

(B) The firing patterns of a CA1 pyramidal cell prior to and during eSWR events. Top three traces recorded from three different tetrodes show a representative eSWR (at the right) event which was preceded by theta oscillation during the 1 s interval prior to eSWR. Raster plot on the bottom shows the firing of cells in consecutive eSWR episodes. Red rasters mark eSWRs events that occurred outside the place field while black ones occurred inside. Note the increased incidence of empty lines outside the place field indicating that in many instances the cell did not fire prior to and during the eSWR event.

(C) The cumulative firing probability function marking the probability of the interval between the time of the last spike before the eSWR and the time of the eSWR onset. The cumulative probability function of different cells was averaged ($n = 151$, mean \pm SEM).

(D) The cumulative probability function marking the probability that different numbers of action potentials occurred before the 1 s periods prior to the SWR event. Results show the averages of different cells ($n = 151$, mean \pm SEM).

(E) Application of temporal sequences of action potentials in CA1 pyramidal neurons derived from in vivo recordings by applying somatic current injections (3 ms, 1–1.5 nA) in vitro recordings. Representative examples with 2, 4, and 6–8 action potentials in the 1 s interval prior to the eSWR (middle panel: “1 s pre SWR interval”). Dendritic spikes were elicited before indicated by “1”) and after the action potential trains (indicated by “2”). Voltage traces (black) and the dV/dt (red) are shown magnified in the rightmost panels. Note potent attenuation of dendritic spikes in all traces in which action potentials were applied.

(F) Quantification of dendritic spike attenuation by the different action potential trains. Attenuation was calculated as the ratio of the maximal $\delta V/\delta t$ of the spikes after and before the train. Error bars indicate standard error of the mean (SEM).

frequency-dependent attenuation of dendritic spikes. This implies an upper limit for the speed at which information stored as compartmentalized differences in branch strength can be retrieved. The frequency-dependent attenuation of dendritic spikes is also interesting in view of the role of dendritic spikes in the induction of plasticity. Dendritic spikes constitute a local associative signal both for synaptic plasticity (Golding et al., 2002; Gordon et al., 2006) as well as for plasticity of branch strength (Losonczy et al., 2008). The dendritic spike attenuation observed at low frequencies predicts that induction of plasticity requiring dendritic spikes would be elicited best by a single stimulus (see Abraham et al., 1986; Holthoff et al., 2004; Remy and Spruston, 2007) or at frequencies at which dendritic spike attenuation is not present (i.e., <1 Hz; Losonczy et al., 2008). These constraints do not apply in the same manner to plasticity elicited with back-propagating action potentials as an associative mechanism for LTP induction (Kampa et al., 2007; Markram et al., 1997), suggesting that two different associative signals in neurons may operate optimally at different frequency ranges. Thus, both storage and readout of information utilizing dendritic-spike-dependent plasticity require sparse neuronal activity.

EXPERIMENTAL PROCEDURES

Slice Preparation and Electrophysiology

Transverse hippocampal slices (300 μ m) were made from 20- to 25-day-old Wistar rats in ice-cold standard artificial cerebrospinal fluid (ACSF) containing (in mM) 125 NaCl, 3.5 KCl, 1.25 NaH_2PO_4 , 26 NaHCO_3 , 2.6 CaCl_2 , 1.3 MgCl_2 , and 15 glucose (95% O_2 / 5% CO_2) by using a vibratome (Leica, Wetzlar, Germany). Before decapitation, deep anesthesia was obtained with ketamine (100 mg/kg, Pfizer, Germany) and xylazine (15 mg/kg, Bayer, Leverkusen, Germany). Slices were incubated at 35°C for 30 min and then held at room temperature for up to 5 hr. Recording temperature in the submerged chamber was 35°C \pm 1°C. Cells were visualized using an Olympus BX-51 epifluorescent microscope equipped with infrared oblique illumination optics and a water immersion lens ($\times 60$, 0.9 NA, Olympus). Somatic whole-cell current-clamp recordings were made in conjunction with a Multiclamp1B amplifier (Molecular Devices, Union City, CA). Data were filtered at 15 kHz and sampled at 100 kHz with a Digidata 1440 interface controlled by pClamp Software (Molecular Devices, Union City, CA). Electrode resistance in the bath ranged from 2 to 3 M Ω , and series resistance ranged from 8 to 20 M Ω . The average membrane resting potential was -60.6 ± 0.3 mV ($n = 145$ cells). In most recordings, the membrane potential was kept slightly hyperpolarized (between -63 and -67 mV) to better isolate the fast spike component from axonal action potentials. The internal solution contained (in mM) 115 K-gluconate, 20 KCl, 10 Na-phosphocreatine, 10 HEPES, 2 Mg-ATP, 0.3 Na-GTP, and 200 μ M Alexa

488 (Molecular Probes) or 200 μM Lucifer yellow (Invitrogen, Carlsbad, CA) to visualize dendritic branches and dendritic spines.

To evoke basal dendritic spikes by local extracellular stimulation, a theta glass pipette was placed near a basal dendrite (40–150 μm from the soma) and a bipolar pulse (biphasic 100–150 μs , 6–65 V, Model 2100, A-M Systems, Sequim, WA) was applied. The stimulation intensity was increased in 5V steps to obtain an input output relationship. If no dendritic spike could be detected at 65V stimulation intensity the stimulating electrode was moved to a different branch. In some experiments the basal dendrite was visualized briefly before recording using epifluorescence (Zeiss HBO 50, 100 μm Alexa 488 in internal solution). In most experiments the basal dendrite was visualized using DIC optics and the fluorescent image was obtained after the experiment to avoid photodamage.

For cell-attached recordings from basal dendrites, slices were perfused with ACSF (33°C), and pipettes were filled with (in mM) 120 NaCl, 3 KCl, 10 HEPES, 2 CaCl₂, 1 MgCl₂, 30 tetraethylammonium chloride (TEA), 5 4-aminopyridine (4-AP), 100 μM Alexa 488 (pH 7.4 with NaOH). Pipettes were fabricated on a vertical puller with a resistance of 7–12 M Ω . Electrodes were coated with sylgard or nail polish to reduce electrode capacitance, and the remaining pipette capacitance was compensated. Membrane potentials were determined by rupturing the patch after the channel data were recorded (–60.4 \pm 3.3mV, $n = 8$). Subsequently, fluorescent dye (Alexa 488) filling of the dendrite and soma was monitored to verify dendritic placement of the recording electrode. Patch currents were recorded using an Axopatch 200B amplifier (Molecular Devices, Union City, CA). Capacitive artifacts were subtracted using a P/4 protocol. Na⁺ currents were elicited with trains of brief depolarizations (Figure 7A, inset), repeated 12 times for averaging. The intertrain interval was 20 s to permit full recovery of Na⁺ channels between trains. No significant rundown of Na⁺ currents was apparent during cell-attached recordings, as shown by analyzing the amplitude of the Na⁺ current elicited by the first depolarization in each of the 12 consecutive stimulus trains (Na⁺ current at the onset of 12th train 107 \pm 8% of the amplitude at onset of the 1st train).

All animal experiments were conducted in accordance with the guidelines of the Animal Care and Use Committee of the University of Bonn.

Multiphoton Uncaging

Two-photon glutamate uncaging at basal dendrites of CA1 pyramidal neurons was performed using a microscope equipped with a galvanometer-based scanning system (Prairie Technologies, Middleton, WI) to photorelease MNI-caged-L-glutamate (Biozol, Eching, Germany; 10 or 15 mM applied via a patch pipette above slice) at multiple dendritic spines. All uncaging locations included in this study were daughter branches bifurcating from a common parent branch, which was directly connected to the 10–30 μm long basal stem. These branches were located \sim 50–120 μm from the soma. Usually 13 spines were selected on a 10–15 μm segment. The minimal distance of the most proximal single uncaging spot to the branch point was 5 μm . Multiphoton photorelease was obtained with an ultrafast, Ti:sapphire pulsed laser (Chameleon Ultra, Coherent) tuned to 725 nm targeted to individual spines with an uncaging dwell time per spine of 1 ms. In some experiments uncaging dwell times of 0.5 ms and 0.2 ms were applied. For uncaging of multiple spines, the laser focus was rapidly moved from spine to spine with a moving time of \sim 0.1 ms. The laser power was kept below 8 mW at the slice surface to avoid photodamage. The experimental approach involved uncaging at individual spines independently (interval >400 ms) to calculate the arithmetic sum of individual events. This expected EPSP was compared to the uEPSP resulting from uncaging at the same set of spines (see Figure 1). Laser power was adjusted to obtain uEPSPs in the range reported for mEPSPs recorded following local application of hyperosmotic solution to basal dendrites (Nevian et al., 2007), mean amplitude of 0.78 \pm 0.03 mV, $n = 108$). This rendered unitary inputs to be easily detectable and stable and allowed to limit the number of uncaging locations to 13 in most recordings. Unitary uEPSPs had 20%–80% rise times of 3.5 \pm 0.1 ms ($n = 108$). As described previously, the unitary uEPSP amplitudes declined with increasing distance of the uncaging site from the soma (Figure S1A), while the 20%–80% rise time increased (Figure S1B; Pearson bivariate correlation coefficient –0.26 and 0.38, respectively, $p = 0.007$ and $p = 0.0001$). Dendritic spikes were also obtained at uncaging sites situated at different distances from the soma. Figure S1C depicts the dependence of

the maximal $\delta v/\delta t$ of dendritic spikes on the distance of the uncaging site from the soma (Pearson bivariate correlation coefficient 0.37, $p = 0.006$ for “weak” branches, strong branches n.s.).

Single-Unit Recording

The surgical and recording procedures, electrode preparation, implantation, and spike-sorting methods have been described previously (O'Neill et al., 2006). Briefly, 14 male rats were implanted with 8–16 independently movable wire tetrodes under deep anesthesia using isoflurane (0.5%–3%), oxygen (1–2 l/min). Tetrodes constructed from four tungsten wires (12 μm in diameter, California Fine Wire, Grover Beach, CA) were attached to microdrives, enabling the independent movement of all the electrodes. The electrode bundles were surgically implanted above the dorsal hippocampus. The head implant was attached to the skull with dental acrylic and stainless-steel screws. After a recovery period of 7 days, the tetrodes were lowered into the hippocampus. Wideband (1 Hz–5 kHz) recordings were taken, and the amplified extracellular field (1000 \times ; via a 64 channel Sensorium [Charlotte, VT] amplifier) and action potentials were digitized continuously at 20 kHz using a 64 channel analog-to-digital converter computer card (United Electronics Industries, Canton, MA). Unit isolation and clustering procedures have been described previously (O'Neill et al., 2006). SWRs were detected by calculating the power (root mean square) of 150–250 Hz band-pass-filtered signal. Detection threshold was set to 7 SD from the baseline mean. SWRs used in this study were detected during exploratory epochs (i.e., eSWRs), which included periods of locomotion or the presence of theta oscillations, including a <2.4 s transient from immobility segments. Those sharp waves that occurred inside and outside the cell's place field were analyzed separately. Locations with firing rates above 20% of the maximum place-rate were marked as inside the place field.

Data Analysis and Statistics

Distance measurements and anatomical evaluation of the dendritic arborization were performed on stacked images collected at the end of recordings using ImageJ (NIH). The distance between the soma and the input site was measured from the center of the soma to the approximate midpoint of the input site in the case of uEPSPs evoked by multisite uncaging. Peak $\delta v/\delta t$ values were obtained from the first derivative of the boxcar-filtered (23 smoothing points) voltage recording. The Kolmogorov-Smirnov normality test and the Dallal and Wilkinson approximation to Lilliefors' method revealed that the $\delta v/\delta t$ value distribution deviates from a normal distribution (KS distance 0.17, $p < 0.0001$). As reported previously in a mixed population of apical and basal branches (Losonczy et al., 2008), a fraction of large-amplitude events lay outside the mean ± 2 standard deviations, indicating more than one underlying distribution. Thus, the data were least-squares fitted using a Levenberg-Marquadt algorithm by the sum of two Gaussian functions in the form of: $Y = ((\text{Area}1/(\text{SD}1*(2*\pi)^{0.5}))*\exp(-0.5*((x-\text{Mean}1)/\text{SD}1)^2)) + ((\text{Area}2/(\text{SD}2*(2*\pi)^{0.5}))*\exp(-0.5*((x-\text{Mean}2)/\text{SD}2)^2))$. The two populations were classified as “weak” ($\delta v/\delta t < 4.8 \text{ V*s}^{-1}$) and “strong” ($\delta v/\delta t > 4.8 \text{ V*s}^{-1}$). The bin size used in the $\delta v/\delta t$ histogram was 0.8 V*s^{-1} . Analysis of electrophysiological data and statistical tests were performed by using IGOR Pro (Wavematrix, Lake Oswego, OR), Excel (Microsoft, Redmond, WA), and Prism4 (GraphPad Software, San Diego, CA). All results are reported as mean \pm SEM, and significance was determined by paired or unpaired two-tailed t tests, unless otherwise indicated.

SUPPLEMENTAL DATA

The Supplemental Data include three figures and can be found with this article online at [http://www.neuron.org/supplemental/S0896-6273\(09\)00156-1](http://www.neuron.org/supplemental/S0896-6273(09)00156-1).

ACKNOWLEDGMENTS

We are grateful to Jason Hardie, Christina Müller and Nelson Spruston for careful reading of the manuscript and Roland Krüppel for technical help. We thank SFB-TR3, BONFOR and the Alexander von Humboldt Foundation for support.

Accepted: January 29, 2009

Published: March 25, 2009

REFERENCES

- Abraham, W.C., Gustafsson, B., and Wigström, H. (1986). Single high strength afferent volleys can produce long-term potentiation in the hippocampus in vitro. *Neurosci. Lett.* **70**, 217–222.
- Ariav, G., Polsky, A., and Schiller, J. (2003). Submillisecond precision of the input-output transformation function mediated by fast sodium dendritic spikes in basal dendrites of CA1 pyramidal neurons. *J. Neurosci.* **23**, 7750–7758.
- Buzsáki, G. (2002). Theta oscillations in the hippocampus. *Neuron* **33**, 325–340.
- Cai, X., Liang, C.W., Muralidharan, S., Kao, J.P., Tang, C.M., and Thompson, S.M. (2004). Unique roles of SK and $K_v4.2$ potassium channels in dendritic integration. *Neuron* **44**, 351–364.
- Cash, S., and Yuste, R. (1999). Linear summation of excitatory inputs by CA1 pyramidal neurons. *Neuron* **22**, 383–394.
- Cheng, S., and Frank, L.M. (2008). New experiences enhance coordinated neural activity in the hippocampus. *Neuron* **57**, 303–313.
- Csicsvari, J., Hirase, H., Mamiya, A., and Buzsáki, G. (2000). Ensemble patterns of hippocampal CA3–CA1 neurons during sharp wave-associated population events. *Neuron* **28**, 585–594.
- Colbert, C.M., Magee, J.C., Hoffman, D.A., and Johnston, D. (1997). Slow recovery from inactivation of Na^+ channels underlies the activity-dependent attenuation of dendritic action potentials in hippocampal CA1 pyramidal neurons. *J. Neurosci.* **17**, 6512–6521.
- Gasparini, S., and Magee, J.C. (2006). State-dependent dendritic computation in hippocampal CA1 pyramidal neurons. *J. Neurosci.* **26**, 2088–2100.
- Gasparini, S., Migliore, M., and Magee, J.C. (2004). On the initiation and propagation of dendritic spikes in CA1 pyramidal neurons. *J. Neurosci.* **24**, 11046–11056.
- Golding, N.L., and Spruston, N. (1998). Dendritic sodium spikes are variable triggers of axonal action potentials in hippocampal CA1 pyramidal neurons. *Neuron* **21**, 1189–1200.
- Golding, N.L., Kath, W.L., and Spruston, N. (2001). Dichotomy of action-potential backpropagation in CA1 pyramidal neuron dendrites. *J. Neurophysiol.* **86**, 2998–3010.
- Golding, N.L., Staff, N.P., and Spruston, N. (2002). Dendritic spikes as a mechanism for cooperative long-term potentiation. *Nature* **418**, 326–331.
- Gordon, U., Polsky, A., and Schiller, J. (2006). Plasticity compartments in basal dendrites of neocortical pyramidal neurons. *J. Neurosci.* **26**, 12717–12726.
- Hoffman, D.A., Magee, J.C., Colbert, C.M., and Johnston, D. (1997). K^+ channel regulation of signal propagation in dendrites of hippocampal pyramidal neurons. *Nature* **387**, 869–875.
- Holthoff, K., Kovalchuk, Y., Yuste, R., and Konnerth, A. (2004). Single-shock LTD by local dendritic spikes in pyramidal neurons of mouse visual cortex. *J. Physiol.* **560**, 27–36.
- Jung, H.Y., Mickus, T., and Spruston, N. (1997). Prolonged sodium channel inactivation contributes to dendritic action potential attenuation in hippocampal pyramidal neurons. *J. Neurosci.* **17**, 6639–6646.
- Kamondi, A., Acsády, L., Wang, X.J., and Buzsáki, G. (1998). Theta oscillations in somata and dendrites of hippocampal pyramidal cells in vivo: activity-dependent phase-precession of action potentials. *Hippocampus* **8**, 244–261.
- Kampa, B.M., and Stuart, G.J. (2006). Calcium spikes in basal dendrites of layer 5 pyramidal neurons during action potential bursts. *J. Neurosci.* **26**, 7424–7432.
- Kampa, B.M., Letzkus, J.J., and Stuart, G.J. (2007). Dendritic mechanisms controlling spike-timing-dependent synaptic plasticity. *Trends Neurosci.* **30**, 456–463.
- Letzkus, J.J., Kampa, B.M., and Stuart, G.J. (2006). Learning rules for spike timing-dependent plasticity depend on dendritic synapse location. *J. Neurosci.* **26**, 10420–10429.
- Losonczy, A., and Magee, J.C. (2006). Integrative properties of radial oblique dendrites in hippocampal CA1 pyramidal neurons. *Neuron* **50**, 291–307.
- Losonczy, A., Makara, J.K., and Magee, J.C. (2008). Compartmentalized dendritic plasticity and input feature storage in neurons. *Nature* **452**, 436–441.
- Magee, J.C., and Carruth, M. (1999). Dendritic voltage-gated ion channels regulate the action potential firing mode of hippocampal CA1 pyramidal neurons. *J. Neurophysiol.* **82**, 1895–1901.
- Markram, H., Lübke, J., Frotscher, M., and Sakmann, B. (1997). Regulation of synaptic efficacy by coincidence of postsynaptic APs and EPSPs. *Science* **275**, 213–215.
- Nevian, T., Larkum, M.E., Polsky, A., and Schiller, J. (2007). Properties of basal dendrites of layer 5 pyramidal neurons: a direct patch-clamp recording study. *Nat. Neurosci.* **10**, 206–214.
- O'Neill, J., Senior, T., and Csicsvari, J. (2006). Place-selective firing of CA1 pyramidal cells during sharp wave/ripple network patterns in exploratory behavior. *Neuron* **49**, 143–155.
- Poirazi, P., and Mel, B.W. (2001). Impact of active dendrites and structural plasticity on the memory capacity of neural tissue. *Neuron* **29**, 779–796.
- Rancz, E.A., and Häusser, M. (2006). Dendritic calcium spikes are tunable triggers of cannabinoid release and short-term synaptic plasticity in cerebellar Purkinje neurons. *J. Neurosci.* **26**, 5428–5437.
- Remy, S., and Spruston, N. (2007). Dendritic spikes induce single-burst long-term potentiation. *Proc. Natl. Acad. Sci. USA* **104**, 17192–17197.
- Schiller, J., Major, G., Koester, H.J., and Schiller, Y. (2000). NMDA spikes in basal dendrites of cortical pyramidal neurons. *Nature* **404**, 285–289.
- Spruston, N., Schiller, Y., Stuart, G., and Sakmann, B. (1995). Activity-dependent action potential invasion and calcium influx into hippocampal CA1 dendrites. *Science* **268**, 297–300.
- Stuart, G., and Häusser, M. (1994). Initiation and spread of sodium action potentials in cerebellar Purkinje cells. *Neuron* **13**, 703–712.
- Stuart, G., Schiller, J., and Sakmann, B. (1997). Action potential initiation and propagation in rat neocortical pyramidal neurons. *J. Physiol.* **505**, 617–632.
- Zhou, W.L., Yan, P., Wuskell, J.P., Loew, L.M., and Antic, S.D. (2008). Dynamics of action potential backpropagation in basal dendrites of prefrontal cortical pyramidal neurons. *Eur. J. Neurosci.* **27**, 923–936.

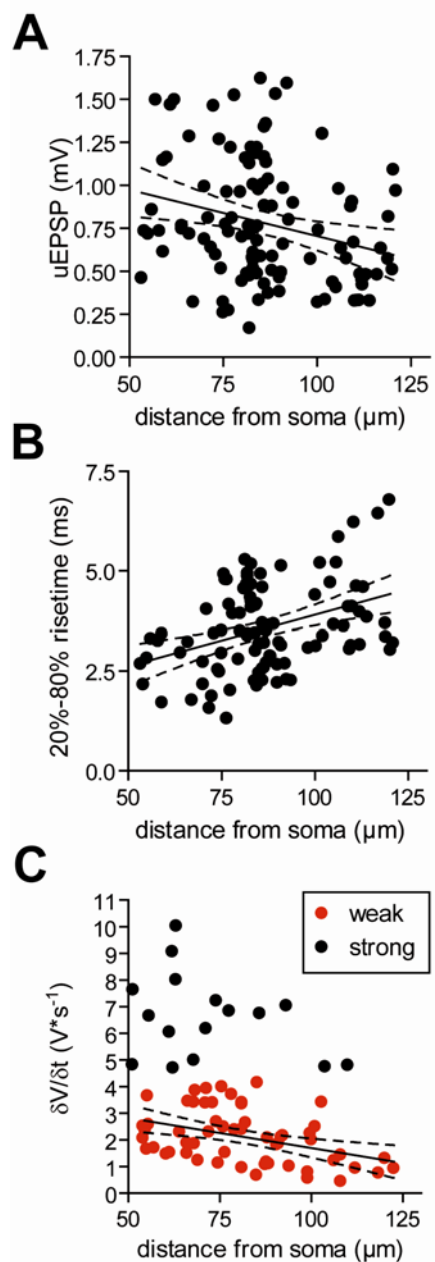
Supplemental Data

Activity-Dependent Control of Neuronal Output

by Local and Global Dendritic Spike Attenuation

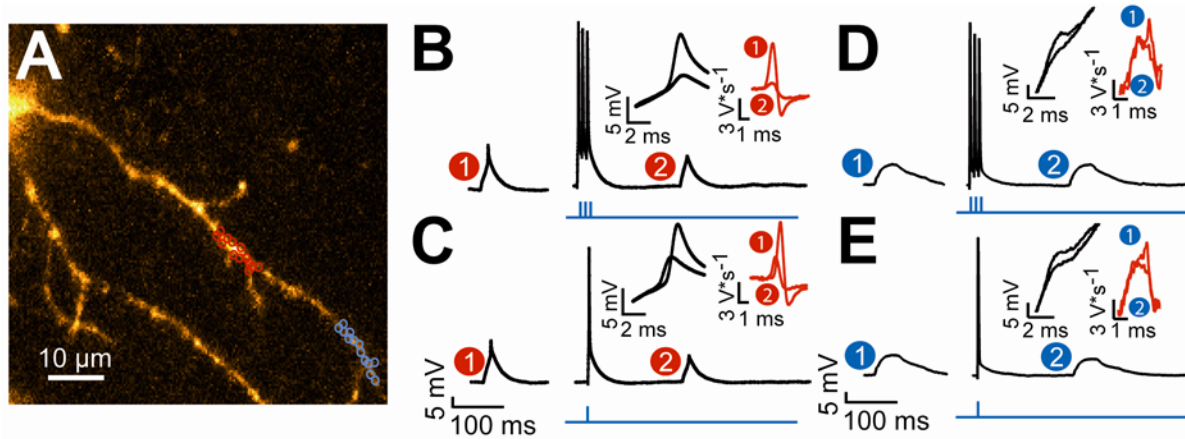
Stefan Remy, Jozsef Csicsvari, and Heinz Beck

Figure S1. Distance Dependence of Unitary uEPSP Properties and Dendritic Spike $\delta V/\delta t$ Values in Basal Dendrites



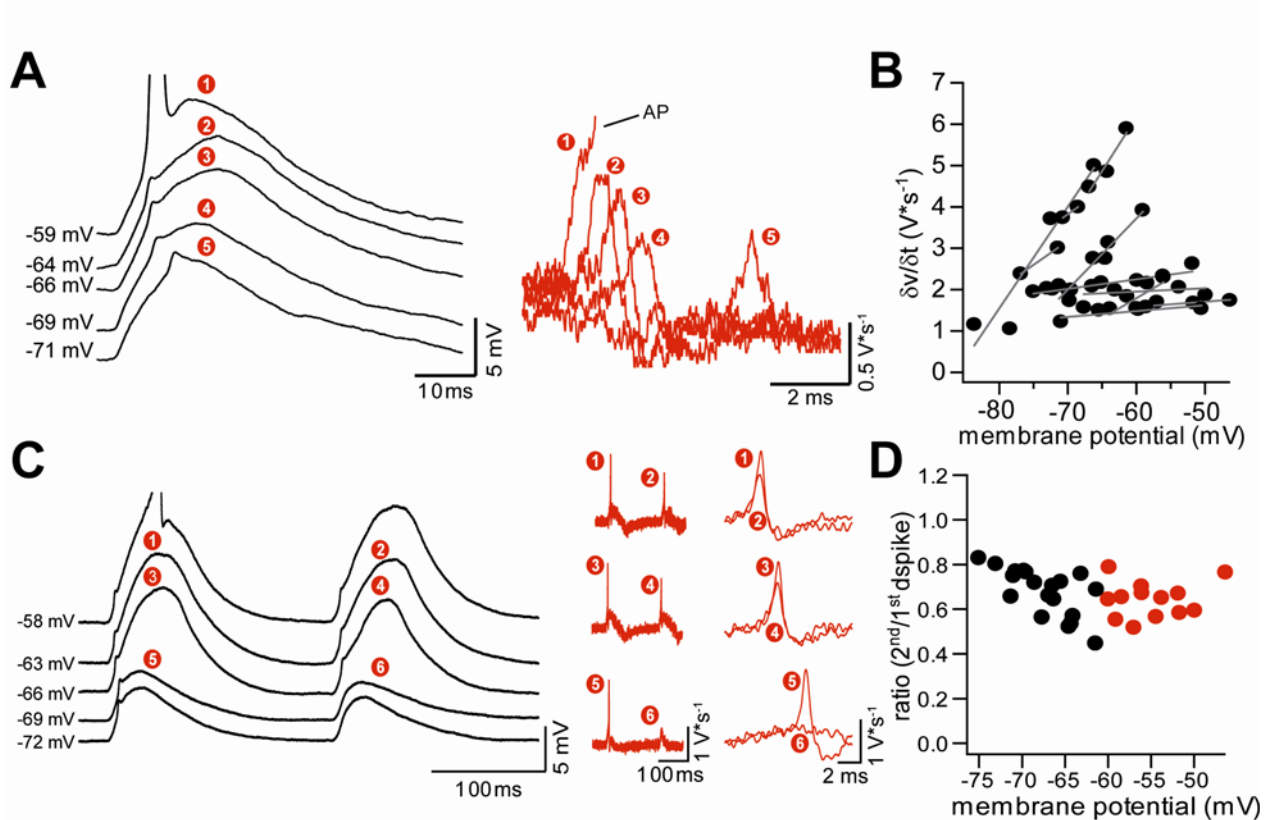
A, Plot of the amplitude of unitary uEPSPs versus distance from the soma. **B**, Plot of the 20-80% uEPSP rise times vs distance from the soma. **C**, Distance dependence of dendritic spike maximal $\delta V/\delta t$ values. 'Strong' and 'weak' branches depicted in black and red, respectively. Plot of uEPSP amplitudes, 20-80% rise times and 'weak' dspike $\delta V/\delta t$ values were fitted with a linear regression (solid line on a, dashed lines represent the 95% confidence interval). For panel c, the fit corresponds to the population of 'weak' branches. For 'strong' branches, no significant correlation of $\delta V/\delta t$ and distance to soma was obtained.

Figure S2. Back-Propagating Action Potentials Attenuate Dendritic Spikes Both at Proximal and Distal Locations on the Same Basal Dendritic Arbor



A, Uncaging locations on proximal (red) and distal (blue) locations. **B**, **C**, Dendritic spike attenuation by action potential bursts (B) or action potentials (C) at the proximal location indicated in panel A. **D**, **E**, Dendritic spike attenuation by action potential bursts (D) or action potentials (E) at distal locations. Insets in panels B-E depict voltage traces (black) and $\delta V/\delta t$ (red) before ('1') and after ('2') action potential firing.

Figure S3. Modest Variation of the Holding Potential Does Not Affect Spike Attenuation



A, Since the dynamics of inactivation and recovery from inactivation of voltage-gated Na^+ channels are voltage-dependent, we tested if varying the holding potential has an effect on spike attenuation. The range within which this could be formally tested was rather small. On the one hand, depolarization eventually caused a somatic action potential to be triggered by the dendritic spike (uppermost trace). On the other hand, hyperpolarization eventually caused spikes to fail, presumably because the local synaptic depolarization no longer reached the dendritic spike threshold. Inset shows dendritic spike $\delta V/\delta t$ at larger magnification. **B**, In each individual experiment, the range over which the effect of varying the membrane potential could be investigated was small (see voltage difference between datapoints linked by red lines, on average 12 ± 2 mV). Depolarizing the membrane potential caused an increase in the dendritic spike $\delta V/\delta t$ in most neurons. In addition, a marked increase of the slow component of the dendritic spike was observed, possibly caused by voltage-dependent augmentation of NMDA receptor-mediated EPSPs (see Fig. S2A, upper vs. lower traces). **C**, Dendritic spike attenuation was not affected by altering membrane potential (red traces show dendritic spike $\delta V/\delta t$ at larger magnification). **D**, Dendritic spike attenuation measured as the ratio of maximal dendritic spike $\delta V/\delta t$ for the second vs. the first stimulation. Black circles: Experiments during which two consecutive dendritic spikes were analyzed. Red circles: Experiments during which the first dendritic spike elicited a somatic action potential. A lack of effect of varying the membrane potential is not surprising since the range within

which we could change membrane potential was small, and is expected to be even smaller at dendritic sites, thus leading only to small changes in the recovery and inactivation rates of dendritic Na⁺ channels.